2D Materials

PAPER

# Van der Waals metallic alloy contacts for multifunctional devices

To cite this article: Kai Xu *et al* 2020 *2D Mater.* **7** 025035

View the article online for updates and enhancements.

This content was downloaded from IP address 98.212.156.85 on 13/04/2020 at 21:03

IOP Publishing 2D Mater. 7 (2020) 025035 https://doi.org/10.1088/2053-1583/ab734d

2D Materials

RECEIVED
29 October 2019

REVISED
27 January 2020

ACCEPTED FOR PUBLICATION
6 February 2020

PUBLISHED
28 February 2020

PAPER

# Van der Waals metallic alloy contacts for multifunctional devices

**Kai Xu, Zijing Zhao, Xiaolin Wu and Wenjuan Zhu**

Electrical and Computer Engineering, University of Illinois at Urbana-Champaign, Urbana, IL 61801, United States of America

**E-mail:** wjzhu@illinois.edu (W Zhu)

**Keywords:** Van der Waals metallic alloy, multifunctional device, $MoTe_2$, $Mo_{1-x}WxTe_2$ alloy

Supplementary material for this article is available online

## Abstract

Two-dimensional (2D) semiconductors have shown great potential for electronic and optoelectronic applications. However, their development is limited by a large Schottky barrier at the contacts because of the strong Fermi-level pinning at the metal-semiconductor interface. Here, we demonstrate that 2D metallic $Mo_{1-x}W_xTe_2$ alloy, bonded to the 2D semiconductor channel $MoTe_2$ via van der Waals (vdW) force, can alleviate the Fermi-level pinning at the contacts. By using asymmetric contacts consisting of low work function Ti and high work function $Mo_{1-x}W_xTe_2$ alloy, ambipolar transistors were created, showing superior transport for both electrons and holes. The $MoTe_2$ transistor with asymmetric contacts is unidirectional and shows prominent rectifying behavior. Moreover, this asymmetric contact scheme breaks the mirror symmetry of the built-in potential profile within the channel, which enables the device to serve as an efficient solar cell and a sensitive photodetector with low dark current. This work uncovers the great potential of 2D metallic contacts for device applications and offers a new route toward tailoring 2D electronics and photonics in the future.

Transistors based on 2D transition metal dichalcogenides (TMDs) offer excellent gate electrostatic control of the channel, which makes them promising candidates for sub-10-nm node technologies [1–12]. In short-channel devices, the transport through the semiconductor is nearly ballistic and the majority of the transistor resistance comes from the contacts. Thus, optimizing the contacts between the TMDs and metal electrodes is a key technical challenge for 2D electronics. In traditional silicon transistors, ohmic contacts are typically achieved by selective ion implantation of the source/drain regions, which can effectively reduce the tunneling barrier width between the metal and the degenerately doped silicon. In 2D TMD transistors, however, ion implantation will induce significant damage to the atomically thin lattice and degrade the current transport. Charge transfer doping and substitutional doping have been explored [13–16]. However, most of these doping methods have limited air stability or thermal stability. Another approach to reduce contact resistance is to minimize the Schottky barrier height. For ideal metal-semiconductor junctions, Schottky barrier height ($\Phi_{SB}$) can be tuned by metal work function based on the Schottky–Mott rule [17, 18]. However, in most TMD-based transistors, the barrier height has very weak dependence on the metal work function due to Fermi-level pinning [19, 20]. To reduce Fermi-level pinning and minimize the Schottky barrier height, various approaches have been investigated. Phase engineering can create lateral metal–semiconductor–metal heterojunctions to reduce the contact resistance, but these heterojunctions have very limited thermal stability [21, 22]. Graphene contacts can provide tunable Schottky barrier height, but cause threshold roll-off [23–26]. Transfer metal to TMDs can eliminate the defects related to metal deposition and provide vdW-like metal/2D interface; however, this method has very limited yield especially for metals with strong adhesion force to the substrates [27]. 2D layers, such as h-BN, were also used as the buffer layers between metal and 2D channel to de-pin the Fermi level [28]. However, due to the insulating nature of the BN layer, the contact resistance is still very high.

In this paper, we design and study 2D metallic alloys as contacts in TMD transistors. These vdW 2D/2D contacts are nearly free of Fermi-level pinning, which enables effective tuning of the Schottky barrier heights. Furthermore, by using asymmetric contact pairs with different work functions, $MoTe_2$

© 2020 IOP Publishing Ltd

transistors with ambipolar transport and unidirectional conduction are demonstrated successfully. We also adopted the asymmetric contact scheme in the photodetectors and solar cells, where the asymmetric contacts break the mirror symmetry of the internal electric field within the channel, allowing for efficient photodetection.

Monolayer $MoTe_2$ and $WTe_2$ have several polymorphs, including semiconducting 1H phase, metallic 1T phase and semi-metallic 1T′ phase [29–35]. For $MoTe_2$ and $WTe_2$, the 1T phase is unstable and is typically turned into distorted 1T′ phase [36–38]. The stacked 1H layers form a three-dimensional bulk with the hexagonal structure ($\alpha$-phase, or 2H phase), while stacked 1T′ layers form a bulk with the monoclinic structure ($\beta$-phase, or T′ phase) or the orthorhombic one ($\gamma$—phase or $T_d$ phase) [36, 39, 40]. For $MoTe_2$, the hexagonal H phase is thermodynamically stable at room temperature, while the monoclinic T′ phase is stable at high temperatures (above 800 °C) [31, 41]. The T′ phase $MoTe_2$ can be stabilized at room temperature by employing special synthesis conditions such as rapid cooling [31, 38]. The T′ phase $MoTe_2$ transitions to $T_d$ phase at low temperatures (250 K–270 K) [31, 42–44]. In contrast, $WTe_2$ has stable $T_d$ phase at room temperature [45, 46]. Alloying $MoTe_2$ and $WTe_2$ can lower the energy barrier between the H, T′ and $T_d$ phases [31, 45]. It is reported that $Mo_{1-x}W_xTe_2$ alloy has T′ phase at $x \leqslant 0.04$, mixed phase ($T' + T_d$) when $0.04 < x < 0.63$.and $T_d$ phase at $x \geqslant 0.63$ [31]. The top view of a 1T′ phase and the side views of $T'$ and $T_d$ phase $Mo_{1-x}W_xTe_2$ are illustrated in figures 1(a) and (b) respectively. To confirm the crystal structure of the $Mo_{1-x}W_xTe_2$ alloys used in our experiments, Raman spectrum was taken on a $Mo_{0.7}W_{0.3}Te_2$ flake, shown in figure 1(c). The peak at 213.6 $cm^{-1}$ corresponds to the $A_1$ vibration mode in $T_d$ phase $WTe_2$ and the peak at 266.6 $cm^{-1}$ corresponds to $A_1$ vibration mode in $T_d$ phase $MoTe_2$, while the peak at 163.4 $cm^{-1}$ corresponds to $A_g$ mode in 1T′ phase $MoTe_2$. The peaks at 79.4 $cm^{-1}$, 108.6 $cm^{-1}$, and 130.7 $cm^{-1}$ can be assigned to either $T_d$ $MoTe_2$ or $T_d$ $WTe_2$. These results are consistent with the mixed phase (1T′ + $T_d$) observed in $Mo_{1-x}W_xTe_2$ alloy with intermediate W composition. The semi-metallic nature of the $Mo_{0.7}W_{0.3}Te_2$ alloy is revealed in the gate voltage and temperature dependence of the drain current in the $Mo_{0.7}W_{0.3}Te_2$ transistor, shown in figure 1(d). The transfer curves of $Mo_{0.7}W_{0.3}Te_2$ transistors measured at 7 K and 280 K show no gate modulation, and the channel resistance decreases with temperature, indicating that this $Mo_{0.7}W_{0.3}Te_2$ flake is metallic. The metallic nature and layered structure of the alloy make it possible to construct vdW metal-semiconductor junctions and enable the effective tuning of Schottky barrier height and carrier polarity.

To facilitate the direct comparison of various contacts, few-layer $MoTe_2$ transistors with two Ti metal contacts and two $Mo_{0.7}W_{0.3}Te_2$ alloy contacts were fabricated on the same flake using photolithography (figure 2(a)). The $MoTe_2$ transistor with two Ti contacts shows strong electron conduction (figure 2(b)), while the transistor with two $Mo_{1-x}W_xTe_2$ contacts exhibits prominent hole conduction (figure 2(c)). More interestingly, the transistor with $Mo_{1-x}W_xTe_2$ as the drain contact and Ti as the source contact displays ambipolar conduction with superior electron and hole conduction simultaneously (figure 2(d)). These phenomena can be explained using the band diagrams shown in figure 2(e). For the transistor with low work function Ti contacts, the Schottky barrier for electron injection is small, while for the transistor with high work function alloy contacts, hole injection dominates. For the transistor with $Mo_{1-x}W_xTe_2$ alloy as the drain contact and Ti as the source contact, the electrons can be injected from the source contact, while holes can be injected from the drain contact, enabling ambipolar transport. The explanations are further confirmed by the reversed condition. If the source and drain contacts are reversed (Ti as the drain contact and alloy as the source contact) and the drain voltage is positive, the transistor shows low current (figure S1). Note that the current flow in FETs with asymmetric contacts is unidirectional (from $Mo_{1-x}W_xTe_2$ contact to Ti contact). This property is reflected in the rectifying output characteristics (figure 2(f)). Thus, by using vdW asymmetric contacts to weaken the Fermi-level pinning, ambipolar $MoTe_2$ transistor and Schottky diode are realized within one device. In addition, compared with the lateral 1T/2H contact, vertical vdW contact can provide larger contact area and van der Waals interface, which can effectively reduce the lattice mismatch induced dislocations and interface state.

To study the barrier height quantitatively, the transport properties of the $MoTe_2$ transistors with metal and alloy contacts at different temperatures were conducted (figures 3(a) and S2). The drain current increases with temperature in both devices. The slopes of the Arrhenius plots (figure 3(b)) in the high-temperature region are analyzed assuming conventional thermionic emission theory $I_d = AA^*T^2 \exp\left(-\frac{\Phi_{SB}}{kT}\right)$, where $I_d$ is the current through the device, $\Phi_{SB}$ is the effective barrier height, $A$ is the junction area, $A^*$ is the Richardson constant, $k$ is the Boltzmann constant and $T$ is the temperature. The extracted $\Phi_{SB}$ is plotted as a function of gate voltage, shown in figure 3(c). In the Ti contact case, when the gate voltage is increased from 15 V to 22.5 V, the effective barrier height for electrons is reduced since the conduction band moves downwards. When the gate voltage is beyond the flatband voltage (~22.5 V), in addition to the thermal excitation of electrons 'over' the Schottky barrier, thermally assisted tunneling 'through' the Schottky barrier will start to contribute to the total current. As a result, the linear dependence between $\Phi_{SB}$ and $V_{gs}$ no longer prevails. From the turning point of the $\Phi_{SB}$ versus gate voltage curves, we can determine the flabtband voltage and the Schottky barrier height. The results are shown in the

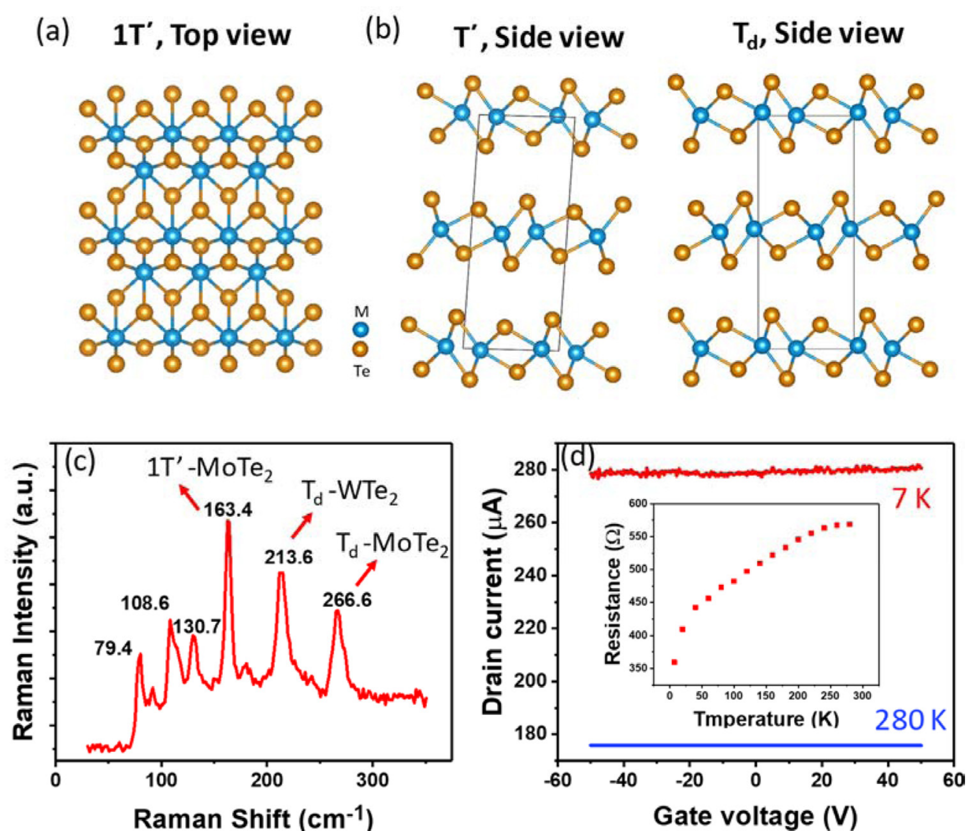


**Figure 1.** Characterization of $Mo_{1-x}W_xTe_2$ ($x = 0.3$). (a) Top view of 1T′phase monolayer $Mo_{1-x}W_xTe_2$. (b) Side views of $T'$ and $T_d$ phase multilayer $Mo_{1-x}W_xTe_2$. $T'$ structure is monoclinic with space group $P2_1/m$, while $T_d$ structure is orthorhombic with space group $Pnm2_1$. (c) Raman spectrum of $Mo_{1-x}W_xTe_2$ alloy with $x = 0.3$. (d) Transfer curves of $Mo_{0.7}W_{0.3}Te_2$ transistors measured at 7 K and 280 K show no gate modulation of drain current, demonstrating metallic properties. The temperature dependence of the channel resistance is shown in the inset.

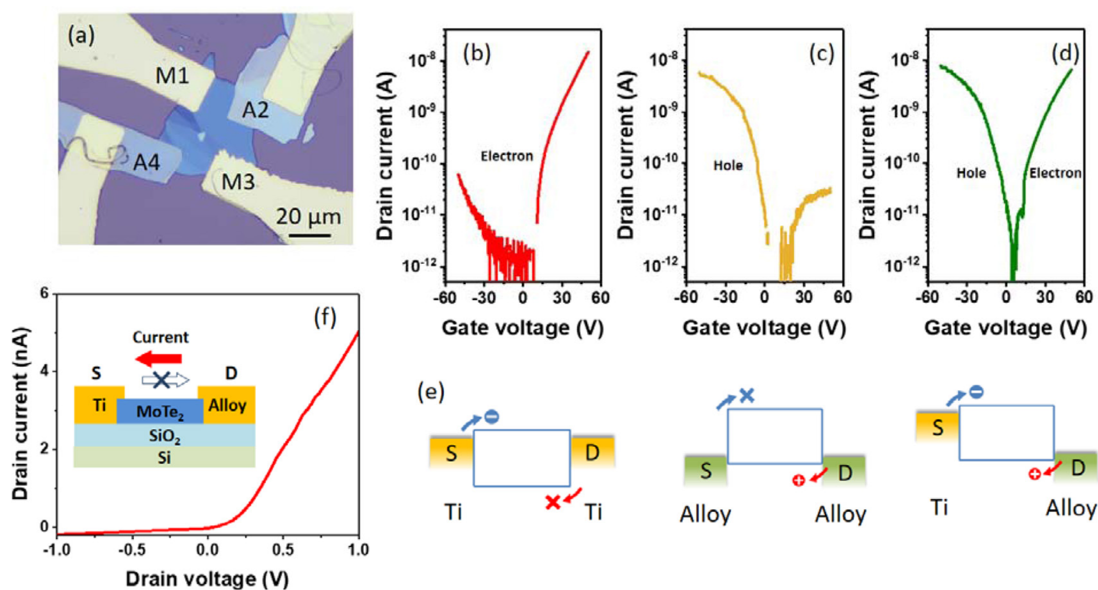


**Figure 2.** Few-layer $MoTe_2$ FETs with two Ti metal contacts and two $Mo_{0.7}W_{0.3}Te_2$ alloy contacts. (a) Optical image of the device. (b)–(d) Transfer curves of the $MoTe_2$ transistors with two Ti contacts, two alloy contacts and asymmetric metal/alloy contacts, respectively. The transistor with alloy as the drain contact and Ti as the source contact displays ambipolar conduction with superior electron and hole conduction simultaneously (e) Energy diagrams of the $MoTe_2$ transistor with these three types of contacts. For transistor with asymmetric contacts, both electrons and holes have low injection barriers. (f) The current flow in the transistor with asymmetric contact is unidirectional (from $Mo_{1-x}W_xTe_2$ contact to Ti contact), as shown in the inset. This property is reflected in the rectifying output characteristics of the transistor.

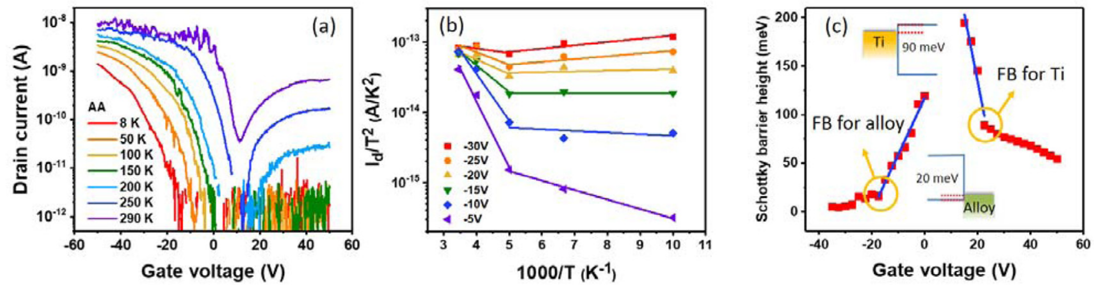


**Figure 3.** (a) Temperature dependence of the drain current for the $MoTe_2$ transistor with alloy contacts. (b) Arrhenius plots of the drain current. (c) Effective barrier heights were extracted at various gate voltages. Schottky barrier heights at the flatband voltage were estimated to be ~20 meV for holes in transistor with alloy contacts and ~90 meV for electrons in transistor with Ti contacts.

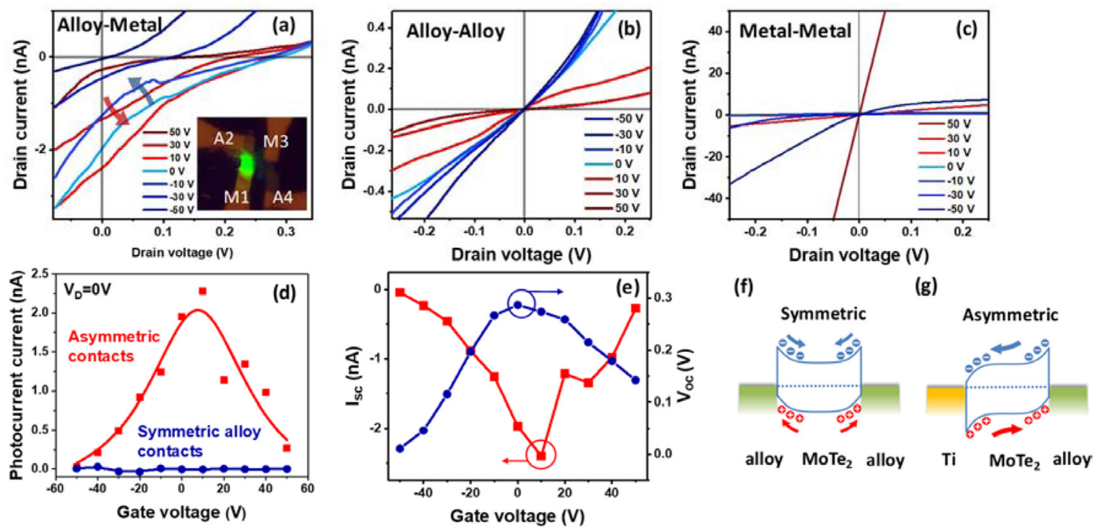


**Figure 4.** $MoTe_2$ phototransistor with asymmetric contacts. (a)–(c) Output curves at various gate voltages under 532 nm laser illumination measured in $MoTe_2$ transistors with asymetric metal-alloy contacts, symmetric alloy contacts, and symmetric Ti contacts, respectively. Only phototransistor with asymmetric contacts shows photovoltaic effect. (d) Photocurrent as a function of gate voltage for transistors with symmetric and asymmetric contacts under zero drain bias. (e) Open-circuit voltage $V_{oc}$ and short-circuit current $I_{sc}$ are dependent on the gate voltage, reaching the maximum values between 0 V and 10 V. (f) and (g) Energy diagrams of the $MoTe_2$ phototransistors with symmetric and asymmetric contacts at zero gate voltage and zero drain voltage. For asymetric contacts, the built-in electric fields near the two contacts are in the same direction, allowing for the individual photocurrent contributions from each contact to be summed, which leads to an enhancement of overall photocurrent and photovoltaic effect.

inset of figure 3(c). The barrier height for holes at the $Mo_{0.7}W_{0.3}Te_2$ alloy contact is ~20 meV and the barrier height for electrons at the Ti contact is ~90 meV. These results confirm that Ti contact in $MoTe_2$ FETs is appropriate for electron conduction, while the $Mo_{1-x}W_xTe_2$ contact is favorable for hole conduction. The combination of these two types of contacts can facilitate both electron and hole conduction simultaneously.

In addition, this asymmetric contact can also enable high-performance optoelectronic devices. Here, we fabricated $MoTe_2$ phototransistors with various contacts. It is found that the phototransistors with asymmetric contacts exhibit prominent photovoltaic effect, shown in figure 4(a). In contrast, the phototransistors with symmetric contacts (two Ti contacts or two alloy contacts) exhibit no photovoltaic effect (figures 4(b) and (c)). Figure 4(d) indicates the photocurrent as a function of gate voltage for transistors with symmetric and asymmetric contacts under zero drain bias. The photocurrent of the transistor with asymmetric contacts is dramatically higher than that with symmetric contacts. This is because, in the transistors with symmetric contacts, the photocurrents generated around these two contacts have the same magnitude, but opposite polarity. The sum of the two contributions is always close to zero at zero drain bias, illustrated in figure 4(f). In the transistor with asymmetric contacts, however, the built-in potential profile within the channel has broken mirror symmetry, allowing for the individual photocurrent contributions from each contact to be summed, leading to an overall photocurrent and a photovoltaic effect, illustrated in figure 4(g). Moreover, the open-circuit voltages ($V_{oc}$) and short-circuit currents ($I_{sc}$) for the transistor with asymmetric contacts are dependent on the gate voltage, reaching the maximum values at about 0 V (figure 4(e)). As discussed above, the built-in electric fields near the two asymmetric contacts have the same direction at the gate voltage around 0 V, leading to the maximum value of $V_{oc}$ and $I_{sc}$. When 50 V or −50 V is applied on the gate, the electric fields

near the two contacts will have opposite directions; thus, the photocurrents generated at the two contacts will cancel each other and lead to reduction of overall photocurrent. A maximum electrical power output of 0.1 nW is obtained at $V_m = 0.124$ V for the $MoTe_2$ solar cell with asymmetric contacts.

In summary, we show that the 2D metallic alloy can provide pristine vdW contacts that are free of Fermi-level pinning to the semiconducting channel. By using asymmetric contacts consisting of alloy and metals, we demonstrated a unique $MoTe_2$ device which can serve as an ambipolar transistor, a unidirectional diode, a high-efficiency solar cell, and a photodetector with low dark current, concurrently. The high work function metallic $Mo_{1-x}W_xTe_2$ alloy and its vdW bonding to the semiconductor enable a low barrier for hole transport. The asymmetric contacts with two different work functions lead to ambipolar behavior with superior electron and hole conduction simultaneously. Based on the temperature-dependence measurements, we quantitatively analyzed the Schottky barriers for electrons and holes. Schottky barrier of 20 meV was extracted for holes in the alloy contacts, and Schottky barrier of 90 meV was extracted for electrons in the Ti contacts. Moreover, the conduction in the $MoTe_2$ transistors with asymmetric contacts is unidirectional, enabling the devices to serve as gate-tunable rectifiers. By virtue of the asymmetric contacts, $MoTe_2$ phototransistors exhibit prominent photovoltaic effect, which can be attributed to the broken mirror symmetry of the built-in potential profile within the channel. The 2D metallic alloy low-resistance contacts presented here represent a new device paradigm that overcomes a significant bottleneck in the performance of 2D materials as the channel materials in postsilicon electronics. This study also provides a promising route to design ambipolar transistors and high-performance optoelectronic devices based on asymmetric contacts, which will have broad applications in computing, sensing and communications.

## Acknowledgments

The authors would like to acknowledge the support from National Science Foundation (NSF) under Grants ECCS 16-11279 and ECCS 16-53241 CAR, and from Office of Naval Research (ONR) under grant NAVY N00014-17-1-2973.

## ORCID iDs

Kai Xu https://orcid.org/0000-0001-7792-8235
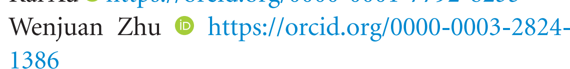
Wenjuan Zhu https://orcid.org/0000-0003-2824-1386


## References


[1] Cao W, Jiang J K, Xie X J, Pal A, Chu J H, Kang J H and Banerjee K 2018 *IEEE Trans. Electron Devices* **65** 4109–21
[2] Mas-Ballesté R, Gómez-Navarro C, Gómez-Herrero J and Zamora F 2011 *Nanoscale* **3** 20–30
[3] Miró P, Audiffred M and Heine T 2014 *Chem. Soc. Rev.* **43** 6537–54
[4] Das S, Robinson J A, Dubey M, Terrones H and Terrones M 2015 *Ann. Rev. Mater. Res.* **45** 1–27
[5] Butler S Z *et al* 2013 *ACS Nano* **7** 2898–26
[6] Chen P, Zhang Z, Duan X and Duan X 2018 *Chem. Soc. Rev.* **47** 3129–51
[7] Chhowalla M, Shin H S, Eda G, Li L-J, Loh K P and Zhang H 2013 *Nat. Chem.* **5** 263
[8] Fiori G, Bonaccorso F, Iannaccone G, Palacios T, Neumaier D, Seabaugh A, Banerjee S K and Colombo L 2014 *Nat. Nanotechnol.* **9** 768
[9] Wang Q H, Kalantar-Zadeh K, Kis A, Coleman J N and Strano M S 2012 *Nat. Nanotechnol.* **7** 699
[10] Jariwala D, Sangwan V K, Lauhon L J, Marks T J and Hersam M C 2014 *ACS Nano* **8** 1102–20
[11] Novoselov K S, Mishchenko A, Carvalho A and Castro Neto A H 2016 *Science* **353** aac9439
[12] Zhu W J, Low T, Wang H, Ye P D and Duan X F 2019 *2D Mater.* **6** 032004
[13] Fang H, Chuang S, Chang T C, Takei K, Takahashi T and Javey A 2012 *Nano Lett.* **12** 3788–92
[14] Fang H, Tosun M, Seol G, Chang T C, Takei K, Guo J and Javey A 2013 *Nano Lett.* **13** 1991–5
[15] Yang L M *et al* 2014 *Nano Lett.* **14** 6275–80
[16] Suh J *et al* 2014 *Nano Lett.* **14** 6976–82
[17] Mott N F 1939 *Proc. R. Soc.* A **171** 0027–38
[18] Bardeen J 1947 *Phys. Rev.* **71** 717–27
[19] Das S, Chen H Y, Penumatcha A V and Appenzeller J 2013 *Nano Lett.* **13** 100–5
[20] Yin L, Zhan X Y, Xu K, Wang F, Wang Z X, Huang Y, Wang Q S, Jiang C and He J 2016 *Appl. Phys. Lett.* **108** 193111
[21] Kappera R, Voiry D, Yalcin S E, Branch B, Gupta G, Mohite A D and Chhowalla M 2014 *Nat. Mater.* **13** 1128–34
[22] Cho S *et al* 2015 *Science* **349** 625–8
[23] Liu Y *et al* 2015 *Nano Lett.* **15** 3030–4
[24] Yu Y J, Zhao Y, Ryu S, Brus L E, Kim K S and Kim P 2009 *Nano Lett.* **9** 3430–4
[25] Yang H, Heo J, Park S, Song H J, Seo D H, Byun K E, Kim P, Yoo I, Chung H J and Kim K 2012 *Science* **336** 1140–3
[26] Yu L L *et al* 2014 *Nano Lett.* **14** 3055–63
[27] Liu Y, Guo J, Zhu E B, Liao L, Lee S J, Ding M N, Shakir I, Gambin V, Huang Y and Duan X F 2018 *Nature* **557** 696
[28] Cui X *et al* 2017 *Nano Lett.* **17** 4781–6
[29] Zhang C X *et al* 2016 *ACS Nano* **10** 7370–5
[30] You J-S, Fang S, Xu S-Y, Kaxiras E and Low T 2018 *Phys. Rev.* B **98** 121109
[31] Oliver S M *et al* 2017 *2D Mater.* **4** 045008
[32] Yang H, Kim S W, Chhowalla M and Lee Y H 2017 *Nat. Phys.* **13** 1232–2
[33] Ouyang B, Lan G Q, Guo Y S, Mi Z T and Song J 2015 *Appl. Phys. Lett.* **107** 191903
[34] Lin X *et al* 2017 *Nat. Mater.* **16** 717
[35] Liu L N *et al* 2018 *Nat. Mater.* **17** 1108
[36] Kim H J, Kang S H, Hamada I and Son Y W 2017 *Phys. Rev.* B **95** 181801
[37] Qian X F, Liu J W, Fu L and Li J 2014 *Science* **346** 1344–7
[38] Keum D H *et al* 2015 *Nat. Phys.* **11** 482–U144
[39] Brown B 1966 *Acta Crystallogr.* **20** 268–74
[40] Dawson W G and Bullett D W 1987 *J. Phys. C: Solid State* **20** 6159–74
[41] Kolobov A V, Fons P and Tominaga J 2016 *Phys. Rev.* B **94** 094114
[42] Yu Q-H, Wang Y-Y, Xu S, Sun L-L and Xia T-L 2016 *Europhys. Lett.* **115** 37007
[43] Hughes H P and Friend R H 1978 *J. Phys. C: Solid State* **11** L103–5
[44] Clarke R, Marseglia E and Hughes H P 1978 *Phil. Mag.* B **38** 121–6
[45] Duerloo K-A N and Reed E J 2016 *ACS Nano* **10** 289–97
[46] Lee C H, Cruz-Silva E, Calderin L, Nguyen M A T, Hollander M J, Bersch B, Mallouk T E and Robinson J A 2015 *Sci. Rep.* **5** 10013